Progress in Nonlinear Differential Equations
and Their Applications, Vol. 64, 357–371

Finite Element Methods for Investigating the Moving Boundary Problem in Biological Development

Cornel Marius Murea and George Hentschel

Abstract. We describe two finite element algorithms which can be used to study organogenesis or organ development during biological development. Such growth can often be reduced to a free boundary problem with similarities to two-fluid flow in the presence of surface tension, though material is added at a constant growth rate to the developing organ. We use the specific case of avian limb development to discuss our algorithms.

1. Introduction

Biological development involves both growth and changes of form which can often involves free moving boundaries [22]. Such moving boundary problems are similar in some respects to two fluid flow interfaces such as the Hele-Shaw problem with surface tension also called Mullins-Sekerka problem. In general, however, in contrast to incompressible flows, growth due to mitosis and nutrients ensure that material is constantly being added (and sometimes removed when cell death or apoptosis occurs). In addition, specific boundary conditions (in general different for each organ or cell type considered) will result in a more complex boundary value problem than those studied in Hele Shaw cells. In this paper to be specific we shall consider avian limb development, though we believe that similar finite element algorithms described here will be useful for other problems of organogenesis or organ morphogenesis and biological development.

In this paper we will consider the evolution of two-dimensional moving domains. The more realistic but more complex case of three-dimensional domains separated by two-dimensional interfaces will be described in a future publication. In the case of the avian limb, the ventral-dorsal length scale (back of limb to palm) is normally small compared to the proximal-distal (tip of finger to point at which the limb joins the main body of the organism) or the posterior-anterior distance

(from thumb to little finger) and therefore two-dimensional simulations are quite informative. In addition, at the developmental stage we are interested in, namely the embryo the whole limb which is only of a millimeter in scale, has approximately the shape of an ellipse with boundary $\Gamma_1(t)$ and a boundary $\Gamma_2(t)$ grafted to the trunk of the organism. In general only the growth velocity of $\Gamma_1(t)$ parallel to the gradient of a pressure, while the growth of $\Gamma_2(t)$ can be described by the motion of the joining vertex with the main trunck (in the more complex three-dimensional case this single point becomes a closed one-dimensional contour). The pressure in the limb whose gradient describes the rate of growth of the limb is the solution of a Poisson problem with Dirichlet boundary conditions depending on the curvature of the boundary.

In Section 2 we give a brief description of some relevant aspects of avian limb development. Then in Section 3 we present a mathematical formulation of the resulting free boundary problem.

In Section 4 two algorithms are described to solve numerically integrate the resulting equations of motion and find the dynamical evolution of the interface.

In the first algorithm the boundary of the domain is approached by a polygon and the pressure is computed by a Finite Element Method. The computed pressure is a piecewise linear function, globally continuous. The curvature is computed as the inverse of the ray of the circle passing through three consecutive vertices of the boundary. The gradient of the pressure is then computed in a vertex of the mesh, as a weighted mean of the gradients in the neighborhood triangles. For the time discretization, we use the forward finite difference Euler's scheme. A dynamic mesh technique is used in order to generate a triangular mesh at each time step. Starting from the mesh at the precedent time step and knowing the boundary at the current time step, we generate a mesh by redistributing the interior vertices using an optimization algorithm. The number of the interior vertices are constant. Also the connections of all meshes are the same, i.e., if i, j, k are the vertices of a triangle in the mesh at the precedent time step, these points are the vertices of a triangle in the current mesh.

While in the second algorithm, the boundary is approached by cubic spline interpolation which gives a curve twice continuously differentiable. The curvature is computed using the parametrization of the splines. Again at each time step, a new mesh is generated, but this time, the generation of the current mesh is independent from the previous one.

In Section 5 we describe the numerical tests of our algorithms. Finally in Section 6, we give a brief discussion of the potential of these approaches for studies of organogenesis and biological development.

2. Early avian limb development

Early avian limb development presents a beautiful example of organogenesis and biological pattern formation: Well-defined developmental axes exist which need

to be understood. Limb growth changes the size and shape of internal domains in which biochemical processes occur. Cartilege formation via mesenchymal cell condensation occurs which will later differentiate into bone and form the skeletal limb. Many of these features appear to be robust: if comparisons are made anatomically with such an apparently different vertabrates as chicken and mouse, it is remarkable the extent to which the gross features of patterning observed during development are conserved by evolution. All of which suggests that universal physical mechanisms controlling development exist.

The embryo produces the raw materials (e.g., proteins, polysaccharides, RNAs) for its development from the available nutrients, according to rules embodied in the genetic code; diffusion, spreading, differential adhesion and chemotaxis transport these materials to specific regions of the organism. The mechanical or chemical changes which may take place in the course of the transport (change of concentration, cell shape, adhesiveness and cohesiveness) are signals that often affect the production of the building material itself, that is, gene activity.

In the course of these events cells differentiate and become more specialized. Differentiation involves regulated gene expression, but elaborate interactions among cells determine where and when new genes are expressed. In addition, morphogenetic changes require coordinated cell movement. The formation of the avian limb requires the establishment of proximal-distal positional gradients and transverse periodic modulations of morphogens to control the formation of individual and multiple parallel skeletal elements. These morphogen patterns act on limb mesenchyme to promote the formation of precartilage condensations, and ultimately the chondrocytes that will give rise to the cartilaginous primordia of the limb skeleton, which ultimately are replaced by bone.

In this paper we wish to investigate only one aspect of this morphogenesis. Namely what type of overall shape is to be expected as a result of growth of the developing embryonic limb. To investigate this problem we consider a minimal model which incorporates the key features of this biological growth. Key is the addition of material at a rate S to the extracellular matrix in which the cells move (more generally the rate of growth will be $S(\mathbf{x}, t)$ as it could be both spatially varying and have a temporal dependence due to genetic switching mechanisms). This means that that the material flow in the limb will obey

$$\nabla \cdot \mathbf{v} = S. \tag{1}$$

We treat growth of the limb as due to a creeping flow because of the very low Reynolds numbers involved [8]. Therefore we can expect the flow to obey Darcy's Law

$$\mathbf{v} = -\alpha \nabla p \tag{2}$$

where p is a pseudo pressure field, which obeys $\Delta p = -S/\alpha$ in the limb domain.

Finally we need biologically reasonable boundary conditions. As it appear there is no flow of material into the main body of the organism at $\Gamma_2(t)$ we shall

take slip boundary condition here

$$\mathbf{v} \cdot \nu = 0, \tag{3}$$

where ν is the outer unit normal vector to the boundary, while the elastic properties of the epithelial layer of cells forming the skin layer at $\Gamma_1(t)$ will result a pressure at this boundary obeying

$$p = \gamma\kappa, \tag{4}$$

where γ is the effective surface tension of the limb [9] while κ is the limb curvature.

The equation of the normal velocity of the boundary $\Gamma_1(t)$ is

$$V_\nu = \mathbf{v} \cdot \nu. \tag{5}$$

The above condition requires that the boundary $\Gamma_1(t)$ moves with the fluid.

It is the integration of this free boundary value problem that we study below. This mathematical model agrees favorably with the analysis presented in [3] based on biological experiments where the limb is considered as a homogeneous and highly hydrated core embedded in an dense envelope.

3. The free boundary problem

We study the evolution of a bounded connected open domain $\Omega(t)$ of $\mathbb{R}^2$ with boundary $\partial\Omega(t) = \Gamma_1(t) \cup \Gamma_2(t)$, where $\Gamma_1(t)$ and $\Gamma_2(t)$ are two non-empty subsets of $\partial\Omega(t)$. Here $t \geq 0$ is the time. We assume that $\Gamma_1(t)$ is a non-closed curve of class $\mathcal{C}^2$ and its ends evolve on the Oy ax. The boundary $\Gamma_2(t)$ is the segment which has the same ends as $\Gamma_1(t)$. Let ν denote the outer unit normal vector to the boundary.

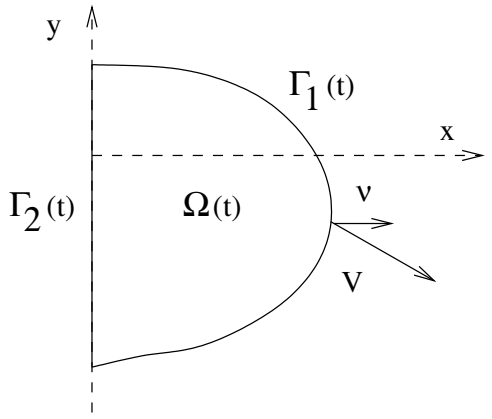

FIGURE 1. Schematic illustration of the free boundary problem

From the equations (1)–(5), we can eliminate $\mathbf{v}$ and we obtain a system in p only. In the moving domain $\Omega(t)$, we have to find the pressure $p(x, y, t) : \Omega(t) \to \mathbb{R}$, such that

$$\begin{cases} -\Delta p &= S/\alpha & \text{in } \Omega(t) \\ p &= \gamma\kappa & \text{on } \Gamma_1(t) \\ \dfrac{\partial p}{\partial \nu} &= 0 & \text{on } \Gamma_2(t) \end{cases} \tag{6}$$

where α, γ, S are positive real constants and κ is the curvature of $\Gamma_1(t)$. We use the sign convention that convex domains have positive curvature of the boundary.

The boundary $\Gamma_1(t)$ evolves according to the law

$$V_\nu = -\alpha \frac{\partial p}{\partial \nu} \tag{7}$$

where V_ν is the normal velocity of $\Gamma_1(t)$.

We know the initial domain

$$\Omega(0) = \Omega^0. \tag{8}$$

We consider the problem (6)–(8) of determining the evolution of $\Omega(t)$ and to find the pressure $p(x, y, t)$ for $t \in [0, T]$, where $T > 0$ is a given real constant.

This problem is similar to the Hele-Shaw problem with surface tension, but in our case the pressure is no longer harmonic ($\Delta p \neq 0$).

Let $\overline{p}(x, y, t) = \frac{S}{4\alpha}\left(x^2 + y^2\right)$. We set $P = p + \overline{p}$ and we obtain from (6)–(7) the following problem: in the moving domain $\Omega(t)$, we have to find the pressure $P(x, y, t) : \Omega(t) \to \mathbb{R}$, such that

$$\begin{cases} \Delta P &= 0 & \text{in } \Omega(t) \\ P &= \gamma\kappa + \overline{p} & \text{on } \Gamma_1(t) \\ \dfrac{\partial P}{\partial \nu} &= 0 & \text{on } \Gamma_2(t) \end{cases} \tag{9}$$

and the normal velocity of the boundary $\Gamma_1(t)$ is

$$V_\nu = -\alpha \left(\frac{\partial P}{\partial \nu} - \frac{\partial \overline{p}}{\partial \nu} \right). \tag{10}$$

Though we cannot prove the existence and uniqueness of our solution, the existence and uniqueness of classical solution for the Hele-Shaw with surface tension problem was proved in [7], suggests that this is the case here also. It is possible that, in order to obtain the existence and uniqueness of solution, we have to prescribe the angles between the boundaries $\Gamma_1(t)$ and $\Gamma_2(t)$. The problem of existence and uniqueness is now under active investigation by G. Simonett.

As it was shown in [12], the shape of the moving domain is determined solely by its normal velocity. In other words, if the velocity of $\Gamma_1(t)$ has the form

$$\mathbf{V} = V_\nu \cdot \nu + V_\tau \cdot \tau$$

where τ is the unit tangent vector to the boundary and V_ν is given by (7), then the movement of the domain and the pressure are the same as in the case $V_\tau = 0$. We set $V_\tau = -\alpha\,(\nabla p \cdot \tau)$ and then $\mathbf{V} = -\alpha \nabla p$. The advantage of this choice is that

we do not need to evaluate the normal vector to the boundary when we compute the velocity of the boundary.

It is convenient to describe the curve $\Gamma_1(t)$ by the parametric coordinates

$$\begin{array}{rcll} x & = & r_1(\theta,t), & \\ y & = & r_2(\theta,t), & \theta \in [a,b]\,. \end{array}$$

Let us introduce the following generalized cylinder:

$$\Omega_T = \bigcup_{t\in]0,T[} \left(\Omega(t)\times\{t\}\right).$$

The problem (6), (7) and (8) is equivalent to the following:
find $r=(r_1,r_2):[a,b]\times[0,T]\to\mathbb{R}^2$ and $p:\overline{\Omega}_T\to\mathbb{R}$, such that

$$\begin{array}{rcll} \dfrac{\partial r_1}{\partial t}(\theta,t) & = & -\alpha\dfrac{\partial p}{\partial x}\left(r_1(\theta,t), r_2(\theta,t), t\right), & \forall\theta\in[a,b], \forall t\in]0,T[\\ \dfrac{\partial r_2}{\partial t}(\theta,t) & = & -\alpha\dfrac{\partial p}{\partial y}\left(r_1(\theta,t), r_2(\theta,t), t\right), & \forall\theta\in[a,b], \forall t\in]0,T[\\ r(\theta,0) & = & \left(r_1^0(\theta), r_2^0(\theta)\right), & \forall\theta\in[a,b] \end{array}$$

where $r^0=\left(r_1^0,r_2^0\right)$ is a parametric representation of $\Gamma_1(0)$ and $p(x,y,t)$ is the solution of (6).

Since $\frac{\partial p}{\partial \nu}=0$ and $\nu=(-1,0)^T$ on $\Gamma_2(t)$, we have $\frac{\partial p}{\partial x}=0$ on $\Gamma_2(t)$. If we suppose that $p\in\mathcal{C}^2(\Omega(t))\cap\mathcal{C}^1\left(\overline{\Omega}(t)\right)$, we obtain that $\frac{\partial p}{\partial x}=0$ at the ends of $\Gamma_2(t)$, also

$$\begin{array}{l} \frac{\partial p}{\partial x}\left(r_1(a,t), r_2(a,t), t\right)=0, \forall t\in]0,T[\\ \frac{\partial p}{\partial x}\left(r_1(b,t), r_2(b,t), t\right)=0, \forall t\in]0,T[. \end{array}$$

Then $\frac{\partial r_1}{\partial t}(a,t)=\frac{\partial r_1}{\partial t}(b,t)=0$ and consequently $r_1(a,t)=r_1(b,t)=0$, $\forall t\in]0,T[$.

The boundary could be parametrized in multiple ways, but the solution must be independent of parametrization.

4. Numerical methods

The free boundary problem (6)–(8) is similar to the Hele-Shaw problem with surface tension also called Mullins-Sekerka problem.

To solve numerically the Hele-Shaw problem with surface tension, there exists an efficient approach named $\theta-L$ introduced in [12]. The variables are the tangent angle θ to the moving boundary and its arc length L. This framework makes the application of an implicit method for time integration easy and it permits to study the problem in a long time interval [13], [4]. In this approach a Fredholm like boundary integral has solved and the integral representation of a harmonic function is used. This is specific to some linear problems with constant coefficients. This method is not appropriate if we replace the linear Darcy's law (2) by the nonlinear Navier-Stokes equation with a volume source located at a certain point in

the domain

$$\rho_0 \left(\frac{\partial \mathbf{v}}{\partial t} + (\mathbf{v} \cdot \nabla) \mathbf{v} \right) - \mu \Delta \mathbf{v} + \nabla p = \mathbf{f} + \frac{\mu}{3} \nabla (\nabla \cdot \mathbf{v})$$

where $\rho_0 > 0$ is the density of the fluid and $\mu > 0$ its viscosity.

A frequented framework used for Navier-Stokes equation in moving domain is Arbitrary Lagrangian Eulerian together with the Finite Element Method [14].

Other approaches are Time-Space Finite Elements [1], Level Set Method [21] and Immersed Boundary Methods [17]. The last one was employed to study the avian limb development in [6]. One of the disadvantage of the continuum models is the complex implementation required to handle the moving boundary of the domain where we have to solve a system of PDEs.

In [15] the software *CompuCell* is presented, where a purely continuum approach for morphogenesis is used in combination with a discrete cellular automata. One of the part of *CompuCell* is based on the cellular Potts model (CMP). A criticism of this formalism is that it neglects simple force balance between cells.

In this paper we present two algorithms which belong to the general framework called "front-tracking methods" [5]. The numerical results were produced for the Darcy's law, but these algorithms could be used for the steady Navier-Stokes equation also.

4.1. The first algorithm

For the time discretization, we use the forward finite differences Euler's scheme. We denote by Δt the time step and by $N = T/\Delta t$ the number of time steps. We approximate $\Gamma_1(n\Delta t)$ by a polygonal line Γ_1^n of vertices (x_i^n, y_i^n) for $i = 0, \ldots, M$. We have $x_0^n = x_M^n = 0$, for all n. We denote by Ω^n the polygonal domain bounded by Γ_1^n and the Oy ax. For each vertex (x_i, y_i) of Γ_1^n, we compute the discrete curvature $\kappa^n(x_i, y_i)$ as the inverse of the ray of the circle passing through the three points (x_{i-1}^n, y_{i-1}^n), (x_i^n, y_i^n) and (x_{i+1}^n, y_{i+1}^n).

The problem (6) is solved numerically by the Finite Element Method. The computed pressure p^n is approached by P_1 function, globally continuous. We follow [18] for computing the discrete gradient of p^n. Let A be a vertex of Γ_1^n. We denote by $star(A)$ the set of all triangles T of the mesh such that A is a vertex of T. We compute the discrete gradient of p^n at the point A as following:

$$\frac{\sum_{T \in star(A)} Area(T) \cdot \nabla p^n{}_{|T}}{\sum_{T \in star(A)} Area(T)},$$

where $p^n{}_{|T}$ is the linear function representing the restriction of the function p^n on the triangle T.

Algorithm 1

Generate a triangular mesh for Ω^0 using **freefem+** [2].
for each n **from** 0 **to** $N-1$ **do**

Step 1: Compute the discrete curvature $\kappa^n(x_i, y_i)$ at each vertex (x_i, y_i) of Γ_1^n.

Step 2: Compute p^n by the Finite Element Method

$$\begin{cases} -\Delta p^n(x,y) &= S/\alpha, & \text{in } \Omega^n \\ p^n(x_i,y_i) &= \gamma\,\kappa^n(x_i,y_i), & \forall\,(x_i,y_i) \text{ vertex of } \Gamma_1^n \\ \dfrac{\partial p^n}{\partial \nu}(x,y) &= 0, & \text{on } \Gamma_2^n. \end{cases}$$

Step 3: Compute the discrete gradient of p^n at each vertex of Γ_1^n.

Step 4: Compute the vertices of Γ_1^{n+1}

$$\begin{aligned} x_i^{n+1} &= x_i^n - \alpha\Delta t\frac{\partial p^n}{\partial x}(x_i^n,y_i^n) \\ y_i^{n+1} &= y_i^n - \alpha\Delta t\frac{\partial p^n}{\partial y}(x_i^n,y_i^n) \end{aligned}$$

for each vertex $(x_i^n,y_i^n)\in\Gamma_1^n$, $i=0,1,\ldots,M$, then set $x_0^{n+1}=x_M^{n+1}=0$.

Step 5: The boundary Γ_2^{n+1} is the segment of ends $\left(x_M^{n+1},y_M^{n+1}\right)$ and $\left(x_0^{n+1},y_0^{n+1}\right)$.

Step 6: Compute a triangular dynamic mesh for Ω^{n+1}, where $\partial\Omega^{n+1}=\Gamma_1^{n+1}\cup\Gamma_2^{n+1}$ using the algorithm [16].

endfor;

At the **Step 6**, we start from the mesh at the precedent time step and knowing the boundary at the current time step, we generate a mesh by redistributing the interior vertices using an optimization algorithm. The number of the interior vertices are constant. Also, the connections of all meshes are the same, i.e., if i, j, k are the vertices of a triangle in the mesh at the precedent time step, these points are the vertices of a triangle in the current mesh.

4.2. The second algorithm

Let (x_i^n,y_i^n) for $i=0,\ldots,M$ be points on $\Gamma_1(n\Delta t)$. Let $\{a=s_0<s_1<\cdots<s_M=b\}$ be a partition of an interval $[a,b]$. We will compute the interpolating cubic spline functions $\Gamma_1^n=\{(x(s),y(s)),\ s\in[a,b]\}$ with the properties:

- $x(s)$ and $y(s)$ are twice continuously differentiable on $[a,b]$,
- $x(s)$ and $y(s)$ coincide on every subinterval $[s_i,s_{i+1}]$, $i=0,\ldots,M-1$ with polynomials of degree three,
- $x(s_i)=x_i^n$ and $y(s_i)=y_i^n$ for $i=0,\ldots,M$,
- $x''(a)=x''(b)=0$ and $y'(a)=y'(b)=0$.

For the numerical tests, we have chosen $s_i=i$, for $i=0,\ldots,M$.
In order to prevent the oscillations, we could choose $a=0$ and

$$s_{i+1}-s_i=\sqrt{\left(x_i^n-x_{i+1}^n\right)^2+\left(y_i^n-y_{i+1}^n\right)^2}.$$

The curve $(x(s), y(s))$, $s \in [a, b]$ has a continuous curvature given by

$$k(s) = \frac{x'(s)y''(s) - x''(s)y'(s)}{\left((x'(s))^2 + (y'(s))^2\right)^{3/2}}. \tag{11}$$

Algorithm 2

Let (x_i^0, y_i^0) for $i = 0, \ldots, M$ be points on $\Gamma_1(0)$.
for each n **from** 0 **to** $N-1$ **do**

Step 1: Compute the cubic spline functions

$$\Gamma_1^n = \{(x(s), y(s)),\ s \in [a, b]\}$$

Step 2: Compute the curvature $\kappa^n(x_i, y_i)$ at each vertex (x_i^n, y_i^n) using (11).

Step 3: Generate a triangular mesh for Ω^n using **freefem+** [2], where $\partial\Omega^n = \Gamma_1^n \cup \Gamma_2^n$ and Γ_2^n is the segment of ends (x_M^n, y_M^n) and (x_0^n, y_0^n).

Step 4: Step 5: Step 6: Compute p^n, ∇p^n and (x_i^{n+1}, y_i^{n+1}) as in the Algorithm 1.

endfor;

At he step **Step 3**, the generation of the current mesh is independent from the previous one.

We shall now describe some numerical tests of the efficacy of these algorithms in studies of organogenesis.

5. Numerical tests

5.1. The initial domain is a semicircle

First let consider the case where the initial domain is a semicircle of ray R_0. Then, if we set the parametric representation of $\Gamma_1(0)$ as

$$\begin{array}{rcll} r_1^0(\theta) & = & R_0\cos(\theta), & \\ r_2^0(\theta) & = & R_0\sin(\theta), & \theta \in \left[-\dfrac{\pi}{2}, \dfrac{\pi}{2}\right] \end{array}$$

the evolution of the boundary $\Gamma_1(t)$ is described by

$$\begin{array}{rcll} r_1(\theta, t) & = & R_0\, e^{\frac{St}{2}}\cos(\theta), & \\ r_2(\theta, t) & = & R_0\, e^{\frac{St}{2}}\sin(\theta), & \theta \in \left[-\dfrac{\pi}{2}, \dfrac{\pi}{2}\right], \quad t > 0. \end{array}$$

The pressure has the form

$$p\,(x, y, t) = \frac{S}{4\alpha}\left(R_0^2\, e^{St} - x^2 - y^2\right) + \frac{\gamma}{R_0\, e^{\frac{St}{2}}}.$$

The algorithms have been implemented using the programming language C++ and the Finite Element classes of F. Hecht [10]. The numerical results were displayed using `gnuplot`.

The first simulation was performed using the **Algorithm 1** for $R_0 = 1$, $S = 2$, $\gamma = 1$, $\alpha = 0.5$, $\Delta t = 0.05$. The number of time steps is $N = 10$.

A dynamic mesh technique is used in order to generate a triangular mesh at each time step. We have used the algorithm described in [16] for the mesh generation. The initial mesh has: 208 vertices, 362 triangles, $M = 32$ (the number of vertices on the boundary Γ_1), $h = 0.155178$ (the mesh size).

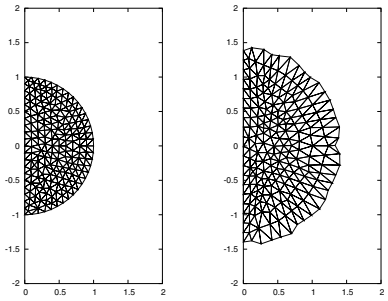

FIGURE 2. The initial mesh (left) and the mesh after 10 time steps (right)

The number of vertices, triangles, boundary edges are the same for the first 10 meshes. In the below table, we see the evolution of the mesh size h.

Time step (n)	1	2	3	4	5
Mesh size (h)	0.155	0.171	0.187	0.202	0.216

Time step (n)	6	7	8	9	10
Mesh size (h)	0.231	0.244	0.256	0.266	0.276

After 10 time steps, the domain might be a semicircle of ray $e^{0.5} \approx 1.648721$.

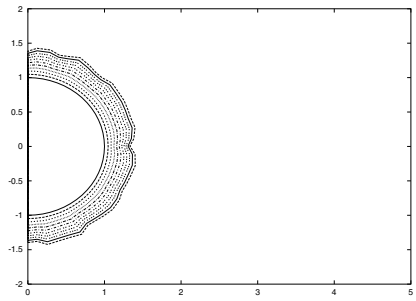

FIGURE 3. The evolution of the moving boundary (0–10 time steps)

The second simulation was performed using the **Algorithm 2** for $\Delta t = 0.0005$ and $N = 1000$ (the number of time steps). The others parameters are the same as in the first simulation.

The software `freefem+` [2] was used to generate a triangular mesh at each time step. The numbers of the vertices and of the triangles are not the same for the all meshes. For example, the mesh after 1000 time steps has 205 vertices and 356 triangles.

After 1000 time steps, the domain might be a semicircle of ray $e^{0.5} \approx 1.648721$.

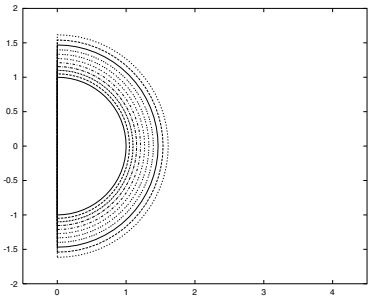

FIGURE 4. The boundary after 0, 100, ..., 1000 time steps

5.2. A non-convex initial domain

Let now consider a case when the initial domain is non-convex as in Figure 5. The boundary $\Gamma_1(0)$ has two flat parts on the bottom, on the top and three semicircles of rays $r1 = 0.6$, $r2 = 0.2$ and $r3 = 0.2$ respectively.

The simulations ware performed for: $S = 2$, $\alpha = 0.5$, $\gamma = 0.5$, $\Delta t = 0.0001$ and $N = 180$ (the number of time steps).

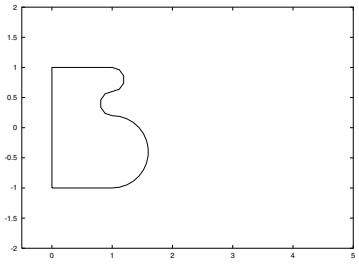

FIGURE 5. The initial domain

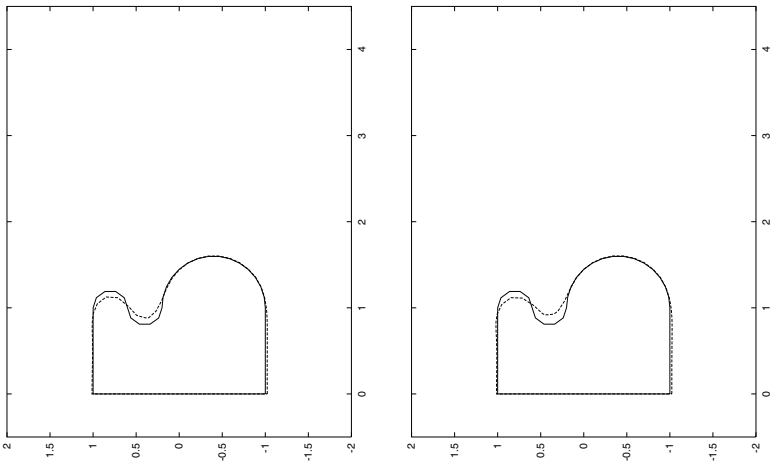

FIGURE 6. The initial (continuous) and the final (dashed) boundaries. Algorithms 1 (left) and 2 (right)

We have observed that the pressure is almost constant near the two flat parts of $\Gamma_1(t)$ and near the largest semicircle. Consequently, these parts of boundary don't move.

We obtain boundary with self-intersection (like the 8) after 182 time steps using the Algorithm 2 and after 230 time steps using the Algorithm 1.

5.3. Concluding remarks

The second algorithm is superior to the first one due in principal to a better approximation of the curvature and a better mesh. We can improve the results by moving the boundary along the normal velocity which preserves a reasonable distribution of the vertices on the boundary. The velocity of the boundary could be computed more accurate by using P2 Finite Element for the pressure. Also adapting mesh techniques could be employed for improving the quality of the mesh.

In the first numerical test, we have solved the free boundary problem until time $t = 0.5$ and in the second, until $t = 0.018$.

We have to use implicit in time algorithms in order to study this kind of free boundary problem in a long time interval. The Arbitrary Lagrangian Eulerian framework together with the Finite Element Method will be employed in a future paper. These methods could be employed for the Navier-Stokes equation with surface tension.

6. Discussion

The algorithms described above could form the basis for many important investigations of organogenesis and biological development in general. Of course they will need to be extended in several directions to give a quantitative picture of how growth and form develops. Obviously highly computationally intensive three-dimensional simulations are necessary. While genetic switching mechanisms will need to be incorporated in order to understand the temporal properties of biological development. But in addition to these questions many other lines of investigation need to be developed.

For example we know that cell condensation and bone development depend on reaction diffusion mechanisms in a progress zone of undifferentiated cells at the tip of the limb. The size of this progress zone can be expected to have a significant impact on the resulting prepattern created in the limb [19, 20, 11]. This is because even at the most basic level the number of standing waves of a heterogeneous distribution of a chemical species formed by a reaction-diffusion mechanism depends both on the scale of the basic pattern (set by the magnitude of the biological parameters) and on the space available for this pattern to develop (set by the domain size). Thus a very question is how the size of this progress zone changes with time? In order to answer this question studies of limb growth will form a vital ingredient.

Another question involves how the skeletal elements themselves, once formed, would influence growth of the developing limb? Fairly significant changes in internal domain organisation occur between early development when the stylopod and zeugopod are created, and later on when the digits appear. This question will require the development of algorithms for complex connected domains in which the skeletal elements create internal boundaries to growth. In addition, the existence of such internal domains will in turn influence reaction-diffusion mechanisms in the interdigital regions. Such reaction-diffusion mechanisms might be relevant to properly controlled cell death leading ultimately to digit formation. The influence will be very dependent on the relative scale of the patterning compared to the size of the interdigital domains.

Clearly these algorithms need to be developed in several directions for studies of biological development and these will be reported in future publications.

Acknowledgments

The authors are very grateful to Professor Stuart A. Newman from the New York Medical College whose questions and comments have contributed to improve the contents of this paper.

References

[1] Bansch E., Finite element discretization of the Navier-Stokes equations with a free capillary surface. *Numer. Math.* **88** (2001) no. 2, 203–235.

[2] Bernardi D., Hecht F., Ohtsuka K., Pironneau O., A finite element software for PDE: freefem+. `http://www-rocq.inria.fr/Frederic.Hecht`

[3] Borkhvardt V.G., Growth and Shaping of the Fin and Limb Buds. *Russian Journal of Developmental Biology*, **31** (2000) no. 3, 154–161.

[4] Ceniceros H.D., Hou T.Y., Si H., Numerical study of Hele-Shaw flow with suction. *Phys. Fluids* **11** (1999) no. 9, 2471–2486.

[5] Crank J., Free and moving boundary problems. The Clarendon Press, Oxford University Press, New York, 1987.

[6] Dillon R., Othmer H.G., A mathematical Model for outgrowth and spatial pattering of the vertebrate limb bud. *J. Theor. Biol.*, **197** (1999) 295–330.

[7] Escher J., Simonett G., Classical solutions for Hele-Shaw models with surface tension. *Adv. Differential Equations* **2** (1997) no. 4, 619–642.

[8] Forgacs G., Foty R.A., Shafrir Y., Steinberg M.S., Viscoelastic properties of living tissues: a quantitative study. *Biophysical Journal* **74** (1998) 2227–2234.

[9] Foty R.A., Pfleger C.M., Forgacs G., Steinberg M.S., Surface tensions of embryonic tissues predict their mutual envelopment behavior. *Development* **122** (1996) 1611–1620.

[10] Hecht F., C++ et Eléments Finis, Cours DEA, Université Paris VI, `http://www-rocq.inria.fr/Frederic.Hecht`

[11] Hentschel H.G.E., Glimm T., Glazier J.A., Newman S.A., Dynamical Mechanisms for Skeletal Pattern Formation in the Avian Limb, *Proc. Royal Soc. B.* **271** (2004) 1713–1722.

[12] Hou T.Y., Lowengrub J.S., Shelley M.J., Removing the stiffness from interfacial flows with surface tension. *J. Comput. Phys.* **114** (1994) 312–328.

[13] Hou T. Y., Lowengrub J. S., Shelley M. J., The long-time motion of vortex sheets with surface tension. *Phys. Fluids* **9** (1997) no. 7, 1933–1954.

[14] Hughes T.J.R., Liu W.K., Zimmermann T.K., Lagrangian-Eulerian finite element formulation for incompressible viscous flows. *Comput. Methods Appl. Mech. Engrg.* **29** (1981) no. 3, 329–349.

[15] Izaguirre J.A., Chaturvedi R., Huang C., Cickovski T., Cof J., Thomas G., Forgac G., Alber M., Hentschel G., Newman S.A., Glazier J.A., COMPUCELL, a multi-model framework for simulation of morphogenesis, *Bioinformatics* **20** (2004) no. 7, 1129–1137.

[16] Murea C.M., Dynamic meshes generation using the relaxation method with applications to fluid-structure interaction problems. *An. Univ. Bucuresti Mat.* **47** (1998) no. 2, 177–186.

[17] Peskin C.S., The immersed boundary method. *Acta Numer.* **11** (2002), 479–517.

[18] Pironneau O., Hecht F., Introduction au Calcul Scientifique en C++, Cours Matrîse de Mathématiques, Ingénierie Mathématique. Université Paris VI, 2000. `http://www-rocq.inria.fr/Frederic.Hecht`

[19] Newman S.A., Frisch H.L., Dynamics of skeletal pattern formation in developing chick limb. *Science* **205** (1979), 662–668.

[20] Newman S.A., Frisch H.L., Percus J.K. On the stationary state analysis of reaction-diffusion mechanisms for biological pattern formation. *J. Theor. Biol.* **134**, (1988) 183–197.

[21] Sethian J. A., *Level set methods: evolving interfaces in geometry, fluid mechanics, computer vision and material science*, Cambridge University Press, 1996.

[22] Wolpert L., Beddington R., Brockes J., Jessell T., Lawrence P., Meyerowitz E., *Principles of Development*. Oxford, New York, Tokyo. Oxford University Press, 1998.

Cornel Marius Murea
Laboratoire de Mathématiques et Applications
Université de Haute-Alsace
4, rue des Frères Lumière
F-68093 Mulhouse Cedex, France
e-mail: c.murea@uha.fr

George Hentschel
Emory University
Department of Physics
Atlanta, GA 30322 USA
e-mail: phshgeh@physics.emory.edu